Progress In Electromagnetics Research M, Vol. 24, 251–264, 2012

A NOVEL RC-FDTD ALGORITHM FOR THE DRUDE DISPERSION ANALYSIS

A. Cala' Lesina*, A. Vaccari, and A. Bozzoli

Renewable Energies and Environmental Technologies (REET), Fondazione Bruno Kessler (FBK-irst), I-38123 Trento, Italy

Abstract—One of the main techniques for the Finite-Difference Time-Domain (FDTD) analysis of dispersive media is the Recursive Convolution (RC) method. The idea here proposed for calculating the updating FDTD equation is based on the Laplace transform and is applied to the Drude dispersion case. A novel RC-FDTD algorithm, that we call modified, is then deduced. We test our algorithm by simulating gold and silver nanospheres exposed to an optical plane wave and by comparing the results with the analytical solution. The modified algorithm guarantees a better overall accuracy of the solution, in particular at the plasmonic resonance frequencies.

1. INTRODUCTION

We focus here on the explicit Finite-Difference Time-Domain (FDTD) numerical solution method of the Maxwell's equations [1, 2], with the Convolutional Perfectly Matched Layer (CPML) boundary conditions formulation [3]. Although some other approaches for the simulation of Drude dispersive media already exist [4–16], we consider the Recursive Convolution (RC) algorithm [17], that we call standard, as reference. It time-discretizes directly the convolution integral expressing the temporal non-locality between the $\mathbf{D}$ and $\mathbf{E}$ fields. In order to minimize the truncation error, we propose here to find a closed form solution of the Ampère-Maxwell equation, and only after to proceed with the time discretization. We calculate explicitly the kernel of such a closed form solution in the case of Drude media deducing the modified RC algorithm, and show how it can be updated recursively with the same memory requirements than the standard RC scheme. The evaluation of some error parameters and the comparison of the electromagnetic fields

Received 19 April 2012, Accepted 23 May 2012, Scheduled 7 June 2012

* Corresponding author: Antonino Cala' Lesina (lesina@fbk.eu).

highlight the better accuracy of the proposed modified RC algorithm with respect to the standard one. The test has been done for Au and Ag noble metals [18] nanospheres, in the optical frequency range, and makes the modified RC algorithm suitable for the simulation of plasmonic resonant nanostructures and optical antennas, as for example proposed in [19, 20].

2. THEORETICAL APPROACH

The temporal non-locality relation between the **D** and **E** fields in dispersive media is expressed by means of the convolution integral

$$\mathbf{D}(t) = \epsilon_0 \epsilon_\infty \mathbf{E}(t) + \epsilon_0 \int_0^t \mathbf{E}(t-\tau)\chi(\tau)d\tau \tag{1}$$

which exhibits a Dirac-delta contribution representing the instantaneous response at the infinite frequency through the (relative) permittivity ϵ_∞ term. In (1) $\chi(\tau)$ is the inverse Fourier transform of the electric susceptibility $\bar{\chi}(\omega)$. This measures the media polarization and enters the complex permittivity $\epsilon(\omega)$ in

$$\mathbf{D}(\omega) = \epsilon_0 \left[\epsilon_\infty + \bar{\chi}(\omega)\right] \mathbf{E}(\omega) = \epsilon(\omega)\mathbf{E}(\omega), \tag{2}$$

i.e., the proportionality coefficient between **D** and **E** in the angular frequency domain ω after a Fourier transform with respect to the time variable. In (2) the same letters are used to denote the fields both in the time and frequency domain and the space dependence is understood. The Ampère-Maxwell equation which is time stepped in the FDTD method, along with the Faraday-Maxwell curl equation for the **E** and **B** fields, is

$$\boldsymbol{\nabla} \times \mathbf{H} = \frac{\partial \mathbf{D}}{\partial t} + \sigma \mathbf{E}, \tag{3}$$

where σ is the static conductivity contribution. Before discretizing (3) for time stepping however, we analytically solve it with respect to the time variable by the Laplace transform method, to get a closed form solution for the electric field **E** at a given time instant t. If we denote by s the dual of the time variable t, omit an understood space dependence as before, and now use a tilde for a Laplace transformed quantity, we have from (1)

$$\tilde{\mathbf{D}}(s) = \epsilon_0 \left[\epsilon_\infty + \tilde{\chi}(s)\right] \tilde{\mathbf{E}}(s) \tag{4}$$

and from (3)

$$\boldsymbol{\nabla} \times \tilde{\mathbf{H}}(s) = s\tilde{\mathbf{D}}(s) - \mathbf{D}(0) + \sigma \tilde{\mathbf{E}}(s), \tag{5}$$

where we assumed that the curl operator $\boldsymbol{\nabla}\times$, acting on the space variables, commutes with the Laplace transform operator. By solving

for $\tilde{\mathbf{D}}(s)$ the first of the two previous equations, inserting the result in the second one, where an initial time zero-field condition has been assumed, and then solving for $\tilde{\mathbf{E}}(s)$ we have

$$\tilde{\mathbf{E}}(s) = \tilde{G}(s) \cdot \boldsymbol{\nabla} \times \tilde{\mathbf{H}}(s), \tag{6}$$

where $\tilde{G}(s)$ stands for

$$\tilde{G}(s) = \frac{1}{s\epsilon_0 \left[\epsilon_\infty + \tilde{\chi}(s)\right] + \sigma}. \tag{7}$$

Note that $\tilde{\chi}(s = -i\omega) = \bar{\chi}(\omega)$ where $i = \sqrt{-1}$ is the imaginary unit. By returning to the time domain through an inverse Laplace transform, we get the aforementioned closed form exact solution for the electric field

$$\mathbf{E}(t) = \int_0^t G(t-\tau) \cdot \boldsymbol{\nabla} \times \mathbf{H}(\tau) d\tau, \tag{8}$$

where the convolutional kernel $G(\tau)$ depends on the medium dispersion characteristic. Note that if in (1) $\chi(\tau)$ were identically zero, we would recover the usual non-dispersive behavior with the absolute dielectric constant $\epsilon = \epsilon_0\epsilon_\infty$. This would imply an identically zero $\tilde{\chi}$ in (7) too. For the corresponding original G we would then get

$$G(\tau) = \frac{1}{\epsilon} e^{-\frac{\sigma}{\epsilon}\tau}, \tag{9}$$

where a Heaviside step function factor of argument is understood. Using this result in (8) and, as is usual in FDTD, sampling at discrete times $n\delta t$, where δt is the time-step, with $\boldsymbol{\nabla} \times \mathbf{H}$ and $\mathbf{H}$ temporally sampled halfway at $(n + 1/2)\delta t$, one gets an updating equation for $\mathbf{E}$ with exponential coefficients

$$\mathbf{E}^{n+1} = e^{-\frac{\sigma\delta t}{\epsilon}} \mathbf{E}^n + \frac{\left(1 - e^{-\frac{\sigma\delta t}{\epsilon}}\right)}{\sigma} \boldsymbol{\nabla} \times \mathbf{H}^{n+\frac{1}{2}}, \tag{10}$$

where superscripts denote time levels. By Taylor expanding to first order the coefficients in (10) with respect to the small quantity $\sigma\delta t/\epsilon$, they equal their FDTD discrete counterparts expanded to the same order. With this in mind we think that our approach based on (8) is less prone to time truncation errors, mainly for highly absorptive media with rapidly time decaying fields, than the standard method based on an early discretization of the convolution integral (1).

We now calculate explicitly the convolutional kernel $\tilde{G}(s)$ shown in (7) in the case of Drude dispersion. This is formulated by the single term electric susceptibility

$$\tilde{\chi}(s) = \frac{\omega_D^2}{s(s+\gamma)}, \tag{11}$$

where ω_D and γ are the plasma frequency and the damping coefficient. This gives

$$\tilde{G}(s) = \frac{s+\gamma}{\epsilon_0\epsilon_\infty(s-s_+)(s-s_-)}, \tag{12}$$

where

$$s_\pm = -P \pm iQ \tag{13}$$

and

$$P = \frac{1}{2}\left(\gamma + \frac{\sigma}{\epsilon_0\epsilon_\infty}\right), \quad Q = \sqrt{\frac{\epsilon_0\omega_D^2 + \sigma\gamma}{\epsilon_0\epsilon_\infty} - P^2} \quad . \tag{14}$$

After returning to the time-domain we get

$$G(\tau) = \frac{1}{\epsilon_0\epsilon_\infty}\left[\frac{e^{s_+\tau}(s_+ + \gamma)}{s_+ - s_-} + \frac{e^{s_-\tau}(s_- + \gamma)}{s_- - s_+}\right] \tag{15}$$

which, putting

$$S = \frac{1}{2}\left(\gamma - \frac{\sigma}{\epsilon_0\epsilon_\infty}\right), \tag{16}$$

has the following form

$$G(\tau) = \Im\left\{Ke^{-W\tau+i\Phi}\right\}, \tag{17}$$

where

$$K = \frac{1}{\epsilon_0\epsilon_\infty}\sqrt{1+\left(\frac{S}{Q}\right)^2}, \tag{18}$$

$$W = P - iQ, \tag{19}$$

$$\Phi = \arctan\frac{Q}{S}, \tag{20}$$

with K and Φ real quantities. $\Re$ and $\Im$ denote the real and imaginary parts of a complex quantity. By defining the complex vector

$$\mathbf{\Psi}(t) = \int_0^t Ke^{-W(t-\tau)+i\Phi} \cdot \boldsymbol{\nabla} \times \mathbf{H}(\tau)d\tau \tag{21}$$

one sees that, according with (8) and (17), the electric field $\mathbf{E}$ results to be

$$\mathbf{E}(t) = \Im\left\{\mathbf{\Psi}(t)\right\} = \int_0^t \Im\left\{Ke^{-W(t-\tau)+i\Phi}\right\} \cdot \boldsymbol{\nabla} \times \mathbf{H}(\tau)d\tau. \tag{22}$$

Sampling (21) at the discrete times $n\delta t$ ($n = 1, 2, \ldots$) we have

$$\mathbf{\Psi}^{n+1} = \int_0^{(n+1)\delta t} Ke^{-W((n+1)\delta t-\tau)+i\Phi} \cdot \boldsymbol{\nabla} \times \mathbf{H}(\tau)d\tau. \tag{23}$$

Separating the integration interval we obtain

$$\begin{aligned}\mathbf{\Psi}^{n+1} &= e^{-W\delta t}\int_0^{n\delta t} Ke^{-W(n\delta t-\tau)+i\Phi}\cdot\boldsymbol{\nabla}\times\mathbf{H}(\tau)d\tau \\ &\quad +\boldsymbol{\nabla}\times\mathbf{H}^{n+\frac{1}{2}}\cdot\int_{n\delta t}^{(n+1)\delta t} Ke^{-W((n+1)\delta t-\tau)+i\Phi}d\tau \end{aligned} \quad (24)$$

and then

$$\mathbf{\Psi}^{n+1} = e^{-W\delta t}\cdot\mathbf{\Psi}^{n} + A\cdot\boldsymbol{\nabla}\times\mathbf{H}^{n+\frac{1}{2}}, \quad (25)$$

where the complex coefficient A is given by

$$A = \int_{n\delta t}^{(n+1)\delta t} Ke^{-W((n+1)\delta t-\tau)+i\Phi}d\tau = K\frac{e^{i\Phi}\left(1-e^{-W\delta t}\right)}{W}. \quad (26)$$

Thus storing, as in the RC traditional scheme [17], one extra complex variable for each sampling point and each electric field component, updating it according to (25), and using its imaginary part as a new electric field value, allows us to include dispersive media in a simpler and more accurate recursive procedure. By expanding the exponential factor according to the Euler formula

$$e^{-W\delta t} = e^{-P\delta t}\cdot[\cos(Q\delta t) + i\sin(Q\delta t)] \quad (27)$$

and taking the imaginary part of both sides of (25) we have the modified form of the electric field updating equation

$$\begin{aligned}\mathbf{E}^{n+1} &= e^{-P\delta t}\sin(Q\delta t)\cdot\Re\{\mathbf{\Psi}^{n}\} \\ &\quad +e^{-P\delta t}\cos(Q\delta t)\cdot\mathbf{E}^{n} + \Im\{A\}\cdot\boldsymbol{\nabla}\times\mathbf{H}^{n+\frac{1}{2}}. \end{aligned} \quad (28)$$

For completeness we report the updating equation of the standard method [17]:

$$\mathbf{E}^{n+1} = C_1\cdot\mathbf{\Phi}^{n} + C_2\cdot\mathbf{E}^{n} + C_3\cdot\boldsymbol{\nabla}\times\mathbf{H}^{n+\frac{1}{2}}, \quad (29)$$

where

$$\mathbf{\Phi}^{n} = C_4\cdot\mathbf{E}^{n-1} + e^{-\gamma\delta t}\cdot\mathbf{\Phi}^{n-1} \quad (30)$$

and

$$C_1 = \frac{1}{\epsilon_0+\chi_0}, \quad (31)$$

$$C_2 = (\epsilon_\infty+\Delta\chi_0)C_1, \quad (32)$$

$$C_3 = \frac{\delta t}{\epsilon_0}C_1, \quad (33)$$

$$C_4 = e^{-\gamma\delta t}\Delta\chi_0, \quad (34)$$

$$\chi_0 = \int_0^{\delta t}\chi(\tau)d\tau, \quad (35)$$

$$\Delta\chi_0 = -\frac{\omega_D^2}{\gamma}\left[1 - e^{-\gamma\delta t}\right]^2. \tag{36}$$

3. SIMULATIONS

To test the modified RC algorithm previously proposed, we apply it to a 96 nm radius nanosphere, made of gold or silver, in a monochromatic light beam. The static conductivity is assumed null. We have tested our modified algorithm in particular for Au at $\lambda = 480$ nm and for Ag at $\lambda = 336$ nm and $\lambda = 380$ nm, i.e., the resonance wavelengths evidenced in Fig. 1 through the extinction coefficient C_{ext} defined in [21]. This coefficient is an efficiency parameter defined as the ratio of the particle cross section over a surface which is the geometrical projection of the particle on a plane perpendicular to the incoming field. The extinction, scattering and absorption coefficients for a spherical particle are:

$$C_{ext} = \frac{2}{r^2k^2}\sum_{m=1}^{\infty}(2m+1)\Re(a_m + b_m), \tag{37}$$

$$C_{sca} = \frac{2}{r^2k^2}\sum_{m=1}^{\infty}(2m+1)\left(|a_m|^2 + |b_m|^2\right), \tag{38}$$

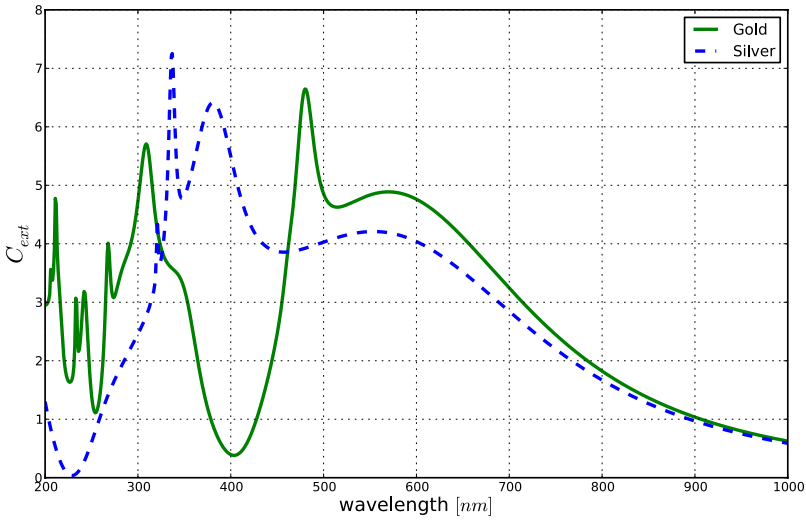

Figure 1. Analytical C_{ext} for Au and Ag nanospheres ($r = 96$ nm) modeled by Drude dispersion.

Table 1. Noble metals drude parameters.

	ϵ_∞	ω_D [rad/s]	γ [s^{-1}]
Au	9.84	$1.3819 \cdot 10^{16}$	$1.09387 \cdot 10^{14}$
Ag	3.70	$1.3521 \cdot 10^{16}$	$3.19050 \cdot 10^{13}$

$$C_{abs} = C_{ext} - C_{sca}, \tag{39}$$

where $k = (2\pi n)/\lambda$, n is the refractive index of the medium surrounding the sphere, λ is the wavelength of the incident radiation, a_n and b_n are combinations of Riccati-Bessel functions [22]. These functions are explicitly dependent on the radius r of the sphere and on the complex dielectric function of the medium. We used a $N \times N \times N$ cubic Yee cell discretization, with $N = 200$, to accommodate the nanosphere. The cell edge (space step $\delta = \delta x = \delta y = \delta z$) amounts to 2 nm for a good representation of the geometrical details. The time step was set to $\delta/(2c_0)$, with c_0 the vacuum light velocity, to satisfy the Courant stability condition [2] in three dimensions. We also used a total field/scattered field (TFSF) source [2], placed 8 cells inward from the outer boundary of the FDTD lattice, to create a plane wave linearly polarized (along the z-axis), impinging along the positive y-direction on the nanostructure. The FDTD lattice was completed with an extra layer, 15 cells thick, supporting the CPML boundary conditions [3] to simulate an open to infinity surrounding media. We used the CPML parameters reported in [23]. We used a compact pulse exciting signal, i.e., of finite duration and with zero value outside a given time interval [24, 25]. The signal duration $T = 1/f_{\max}$ is suitably chosen to get spectral distribution results in the range 200–1000 nm, where $f_{\max}$ is the maximum frequency, as obtained by the Discrete Fourier Transform (DFT) which is updated at every FDTD time iteration, until the excitation is extinguished inside the whole numerical lattice. The excitation signal is $(1 - \cos(\frac{2\pi t}{T}))^3$ and it can be considered extinguished in $3 \div 4$ the time the radiation needs for propagating along the lattice diagonal. The Drude parameters for Au and Ag were taken from the literature [18] and are reported in Table 1.

The electric fields, by means of the DFT, are computed for each sampling point of the lattice at the frequency of interest and are normalized with respect to the incident electric field component at the same frequency. The numerical results for the electric field and the extinction coefficient have been compared with those from the standard RC method [17] through the analytical solutions obtained by implementing the methods described in [21]. The numerical counterpart of C_{ext} is calculated by adding the absorption coefficient

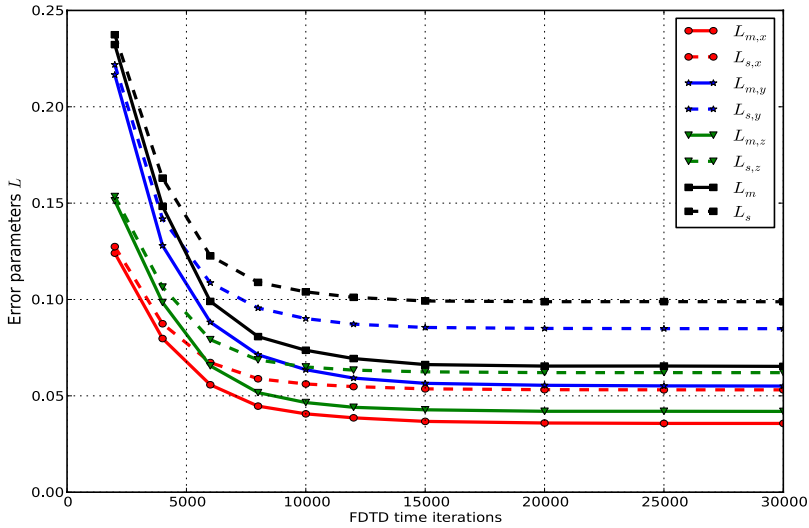

Figure 2. Error parameters $L_{\xi,\eta}$ and L_ξ comparison for Au (DFT at $\lambda = 480\,\text{nm}$).

Table 2. Error evaluation at the resonance frequencies.

	Au (480 nm)	Ag (336 nm)	Ag (380 nm)
$L_{m,x}$ ($L_{s,x}$)	0.0386 (0.0548)	0.1275 (0.1533)	0.0374 (0.0421)
$L_{m,y}$ ($L_{s,y}$)	0.0592 (0.0872)	0.2085 (0.2485)	0.0585 (0.0687)
$L_{m,z}$ ($L_{s,z}$)	0.0440 (0.0633)	0.1718 (0.2024)	0.0430 (0.0478)
L_m (L_s)	0.0693 (0.1011)	0.2670 (0.3282)	0.0594 (0.0684)
LC_m (LC_s)	0.2216 (0.3376)	0.3265 (0.3646)	0.4579 (0.5052)

C_{abs} to the scattering coefficient C_{sca}, indeed only these two are evaluable through a numerical approach. The first is the Poynting vector flux through a closed surface containing the sphere in the total field domain, the second is calculated by means of the same flux through a closed surface located in the scattered field region. In order to evaluate the deviation of the numerical results from the exact solution we considered the average error for each electric field component

$$L_{\xi,\eta} = \frac{1}{N^3} \sum_{i,j,k=1}^{N} \left| E_\eta^\xi(i,j,k) - E_\eta^a(i,j,k) \right|, \tag{40}$$

Table 3. LC_ξ over the total frequency range.

	Au	Ag
LC_m (LC_s)	0.0515 (0.0747)	0.0926 (0.1019)

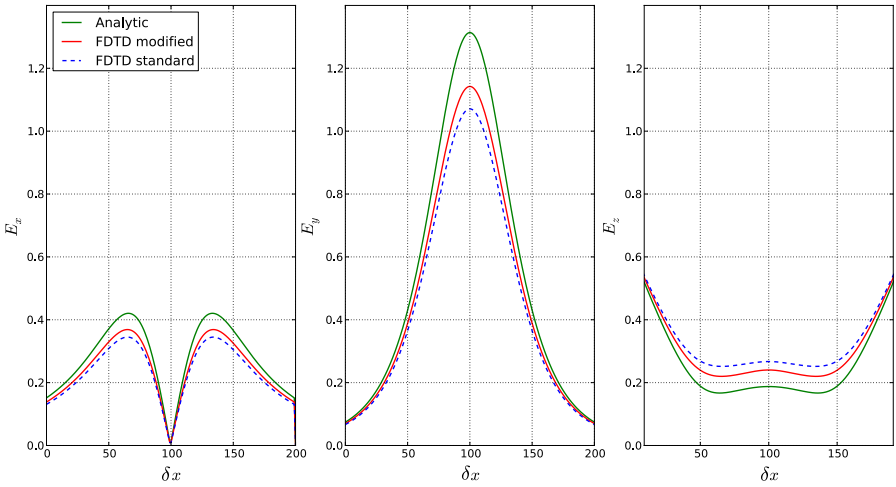

Figure 3. Total field E_x, E_y, E_z for Au nanosphere (DFT at $\lambda = 480\,\text{nm}$) along the x axis ($y = 170$, $z = 120$).

the average error for the electric field module

$$L_\xi = \frac{1}{N^3} \sum_{i,j,k=1}^{N} \left| \left| \mathbf{E}^\xi(i,j,k) \right| - \left| \mathbf{E}^a(i,j,k) \right| \right| \tag{41}$$

and the average error for C_{ext}

$$LC_\xi = \frac{1}{N_\lambda} \sum_{i=1}^{N_\lambda} \left| C^\xi_{ext_i} - C^a_{ext_i} \right|, \tag{42}$$

where $\eta = \{x, y, z\}$ indicates the cartesian component, $\xi = \{s, m\}$, the letters s, m, a denote standard, modified and analytical solution, and N_λ is the number of wavelengths at which C_{ext} has been evaluated. The values in Table 2 were obtained with 12000 time iterations simulations. For the gold resonance the error parameters (40) and (41) are reported as a function of the number of FDTD iterations (Fig. 2). We can observe that the convergence is reached after the same number of FDTD time iterations than in the standard case and in all the cases

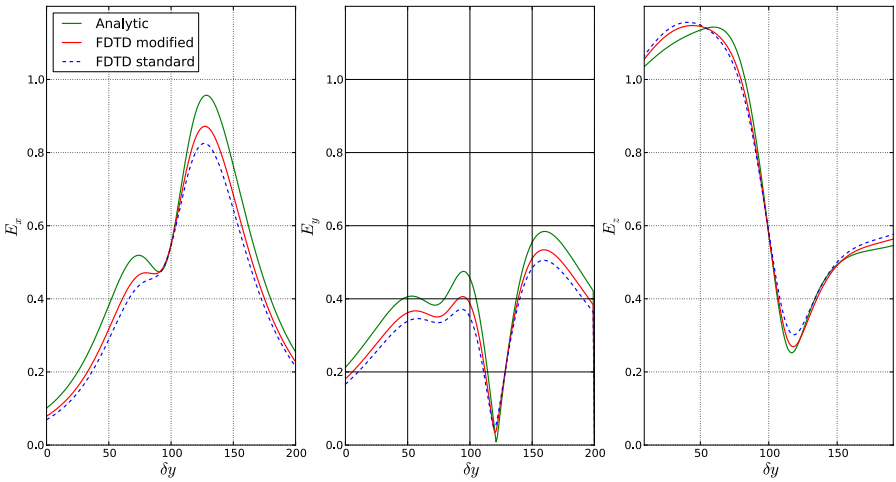

Figure 4. Total field E_x, E_y, E_z for Au nanosphere (DFT at $\lambda = 480\,\text{nm}$) along the y axis ($x = 150$, $z = 150$).

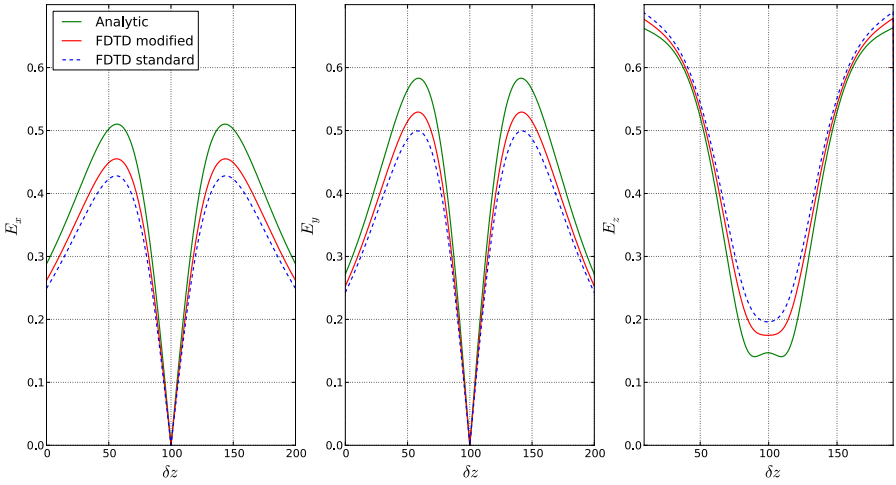

Figure 5. Total field E_x, E_y, E_z for Au nanosphere (DFT at $\lambda = 480\,\text{nm}$) along the z axis ($x = 150$, $y = 170$).

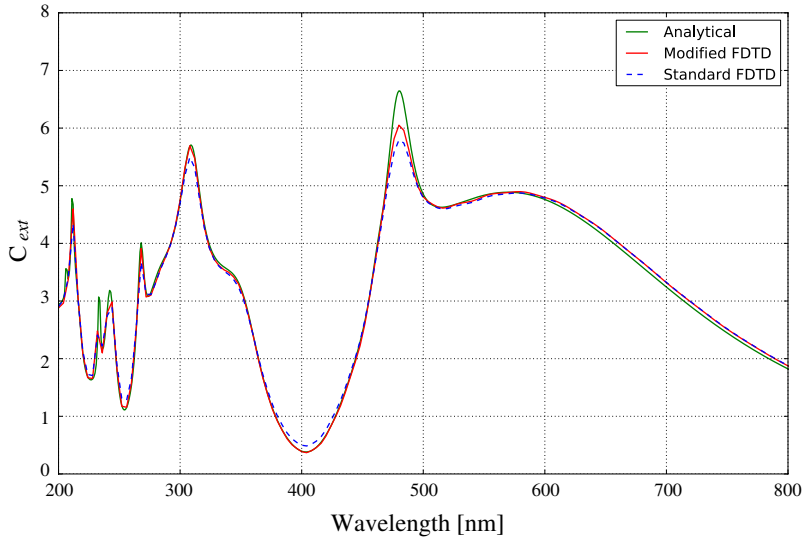

Figure 6. C_{ext} for a gold nanosphere ($r = 96\,\text{nm}$) modeled by Drude dispersion.

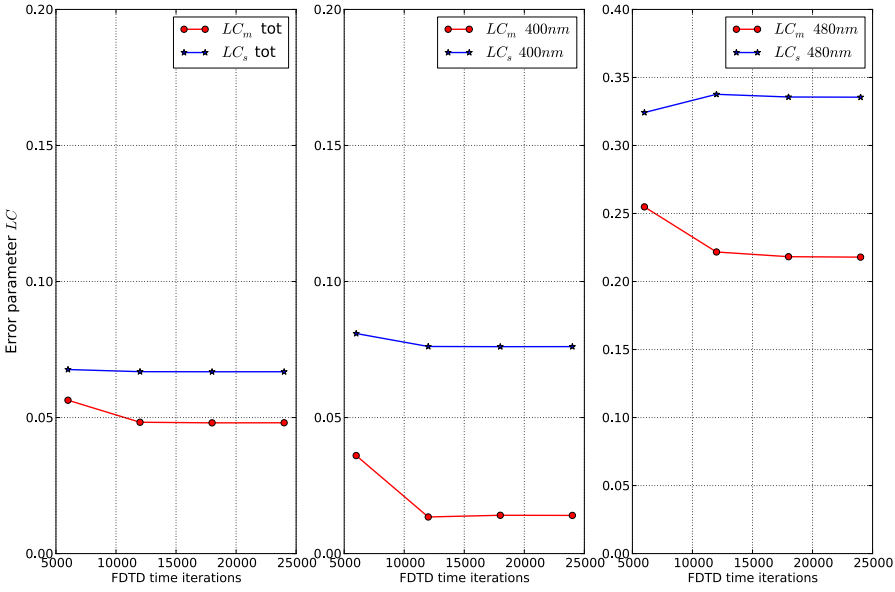

Figure 7. LC_ξ comparison for gold in the total frequency range, and in the region of C_{ext} minimum and maximum.

the level of accuracy is better. The better numerical accuracy is also evidenced with a comparison of the total electric field extracted from the lattice along one direction in x, y and z (Figs. 3–5). In each figure the three components of the electric field (E_x on the left, E_y in the middle and E_z on the right) are represented. The sharp peaks are due to the field inside the sphere, that is very low (metallic sphere), and to some symmetry planes where the field is zero. For gold and silver the extinction coefficient has been calculated and the error parameter (42) at the resonance frequencies (Table 2) and over the total frequency range are reported (Table 3). For gold moreover the C_{ext} comparison is shown in Fig. 6, while in Fig. 7 the error parameter (42) is evaluated for the total frequency range and in the peak regions ($\lambda = 400\,\text{nm}$ and $\lambda = 480\,\text{nm}$) varying the number of time iterations.

4. CONCLUSION

We proposed a modified Recursive Convolution algorithm for the FDTD analysis of Drude dispersive media. The algorithm has been tested by comparing the electric field and the extinction coefficient deviation from the analytical solution for gold and silver nanospheres. It evidences an accuracy improvement with respect to the standard RC method. The better precision is observable in particular at the plasmonic resonance frequencies and makes the modified algorithm suitable for plasmonic simulations.

REFERENCES

1. Yee, K. S., "Numerical solution of initial boundary value problems involving Maxwell's equations in isotropic media," *IEEE Trans. on Antennas and Propagat.*, Vol. 14, No. 3, 302–307, 1966.
2. Taflove, A. and S. C. Hagness, *Computational Electrodynamics: The Finite-difference Time-domain Method*, 3rd Edition, Artech House, Norwood, MA, 2005.
3. Roden, J. A. and S. D. Gedney, "Convolution PML (CPML): An efficient FDTF implementation of the CFS-PML for arbitrary media," *Microwave and Optical Technology Letters*, Vol. 27, No. 5, 334–339, 2000.
4. Sullivan, D. M., "Frequency-dependent FDTD methods using Z transforms," *IEEE Trans. on Antennas and Propagat.*, Vol. 40, 1223–1230, 1992.
5. Gandhi, O. P., B.-H. Gao, and J.-Y. Chen, "A frequency-dependent finite-difference time-domain formulation for general

dispersive media," *IEEE Trans. on Microwave Theory and Tech.*, Vol. 41, 658–665, 1993.

6. Young, J. L., "Propagation in linear dispersive media: Finite difference time-domain methodologies," *IEEE Trans. on Antennas and Propagat.*, Vol. 43, 422–426, 1995.
7. Pereda, J. A., L. A. Vielva, A. Vegas, and A. Prieto, "Statespace approach to the FDTD formulation for dispersive media," *IEEE Trans. on Magn.*, Vol. 31, 1602–1605, 1995.
8. Kelly, D. F. and R. J. Luebbers, "Piecewise linear recursive convolution for dispersive media using FDTD," *IEEE Trans. on Antennas and Propagat.*, Vol. 44, 792–797, 1996.
9. Okoniewski, M., M. Mrozowski, and M. A. Stuchly, "Simple treatment of multi-term dispersion in FDTD," *IEEE Microwave Guided Wave Lett.*, Vol. 7, 121–123, 1997.
10. Chen, Q., M. Katsuari, and P. H. Aoyagi, "An FDTD formulation for dispersive media using a current density," *IEEE Trans. on Antennas and Propagat.*, Vol. 46, 1739–1746, 1998.
11. Pereda, J. A., A. Vegas, and A. Prieto, "FDTD modeling of wave propagation in dispersive media by using the Mobius transformation technique," *IEEE Trans. on Microwave Theory and Tech.*, Vol. 50, 1689–1695, 2002.
12. Okoniewski, M. and E. Okoniewska, "Drude dispersion in ADE FDTD revisited," *Electronics Letters*, Vol. 42, No. 9, 503–504, 2006.
13. Kong, S., J. J. Simpson, and V. Backman, "ADE-FDTD scattered-field formulation for dispersive materials," *IEEE Microwave and Wireless Components Lett.*, Vol. 18, No. 1, 4–6, Jan. 1, 2008.
14. Shibayama, J., et al., "Simple trapezoidal recursive convolution technique for the frequency-dependent FDTD analysis of a drude-lorentz model," *IEEE Photonics Technology Letters*, Vol. 21, No. 2, 100–102, Jan. 15, 2009.
15. Alsunaidi, M. A. and A. A. Al-Jabr, "A general ADE-FDTD algorithm for the simulation of dispersive structures," *IEEE Photonics Technology Letters*, Vol. 21, No. 12, 817–819, Jun. 15, 2009.
16. Zhang, Y.-Q. and D.-B. Ge, "A unified FDTD approach for electromagnetic analysis of dispersive objects," *Progress In Electromagnetics Research*, Vol. 96, 155–172, 2009.
17. Luebbers, R. J., F. Hunsberger, and K.S. Kunz, "A frequency-dependent finite-difference time-domain formulation for transient

propagation in plasma," *IEEE Trans. on Antennas and Propagat.*, Vol. 39, No. 1, 29–34, 1991.

18. Kolwas, K., A. Derkachova, and M. Shopa, "Size characteristics of surface plasmons and their manifestation in scattering properties of metal particles," *Journal of Quantitative Spectroscopy & Radiative Transfer*, Vol. 110, 1490–1501, 2009.
19. Lee, K. H., I. Ahmed, R. S. M. Goh, E. H. Khoo, E. P. Li, and T. G. G. Hung, "Implementation of the FDTD method based on Lorentz-Drude dispersive model on GPU for plasmonics application," *Progress In Electromagnetics Research*, Vol. 116, 441–456, 2011.
20. Paris, A., A. Vaccari, A. Cala' Lesina, E. Serra, and L. Calliari, "Plasmonic scattering by metal nanoparticles for solar cells," *Plasmonics*, 1–10, March 8, 2012.
21. Stratton, J. A., *Electromagnetic Theory*, McGraw-Hill, New York and London, 1941.
22. Bohren, C. F. and D. R. Huffman, *Absorption and Scattering of Light by Small Particles*, Wiley, New York, 1998.
23. Laakso, I., S. Ilvonen, and T. Uusitupa, "Performance of convolutional PML absorbing boundary conditions in finite-difference time-domain SAR calculations," *Phys. Med. Biol.*, Vol. 52, 7183–7192, 2007.
24. Pontalti, R., L. Cristoforetti, and L. Cescatti, "The frequency dependent FD-TD method for multi-frequency results in microwave hyperthermia treatment simulation," *Phys. Med. Biol.*, Vol. 38, 1283–1298, 1993.
25. Vaccari, A., R. Pontalti, C. Malacarne, and L. Cristoforetti, "A robust and efficient subgridding algorithm for finite-difference time-domain simulations of Maxwell's equations," *J. Comput. Phys.*, Vol. 194, 117–139, 2003.